Reconsidering initial Pb in titanite in the context of in situ dating

2 (Revision 1)

- 4 Chloë E. Bonamici*
- 5 Tyler B. Blum
- 6 Department of Geoscience, University of Wisconsin-Madison, 1215 W. Dayton St., Madison,
- 7 WI 53706

Abstract

In situ U-Pb dating of titanite, which can preserve trace-element records of various petrologic processes but also incorporates significant initial Pb, has proliferated in recent years. The widespread use of titanite data to construct tectonic P-T-t paths warrants careful assessment of the available dating techniques, as well as attention to the assumptions that underpin the U-Pb data analysis. This contribution provides the first direct comparison of the two major analytical methods – SHRIMP (SIMS) and LA-ICP-MS – for in situ U-Pb titanite dating. A set of well-characterized titanite grains from Harrisville, NY, in the Adirondack Mountains were analyzed for U-Th-Pb isotopes along the same cross-grain traverses by SHRIMP and LA-ICP-MS. Both LA-ICP-MS and SHRIMP datasets define approximately linear arrays on the Tera-Wasserburg Concordia (semi-total Pb/U) diagram and would commonly be interpreted as representing a single date population with minor scatter. However, previous studies have suggested that Adirondack titanite actually records two regionally well-defined thermal events, ~50-100 m.y.

^{*} Corresponding author. E-mail: <u>bonamici@wisc.edu</u>. Phone: +1 608 263 7754.

apart. When titanite data arrays are treated in detail, attempts to determine concordia-intercept ages by robust three-dimensional linear regression produce large uncertainties and/or poor fit statistics that suggest that the data are not, in fact, isochronous. Grain-by-grain analysis of U-Pb titanite data shows that different subsets of titanite (determined by additional geochemical and microstructural data) show different patterns of U-Pb data. By comparing predictions for Pb-ingrowth evolution paths in Tera-Wasserburg diagrams with observed data, it is possible to recognize both a change in initial Pb composition and Pb loss in the Adirondack titanite U-Pb dataset. This study provides an example of how greater geochronologic detail can be extracted from large *in situ* U-Pb titanite datasets. Even when precise dates are not recovered, geological processes and events that cause data scatter can be recognized through analysis of U-Pb data patterns using the Tera-Wasserburg diagram.

Keywords: titanite; U-Pb geochronology; initial Pb correction; LA-ICP-MS; SHRIMP

1	റ
4	ð

49 Introduction

Titanite is an increasingly popular U-Pb geochronometer and petrogenetic indicator in the 50 study of crystalline rocks (e.g., Aleinikoff et al., 2002; 2004; Chen et al., 2016; Essex and 51 Gromet, 2000; Gao et al., 2012; Garber et al., 2017; Holder and Hacker, 2019; Jung and 52 53 Hellebrand, 2007; Kirkland et al., 2016, 2017; Kohn, 2017; Kohn and Corrie, 2011; Li et al., 2010; Marsh and Smye, 2017; Olierook et al., 2019; Papapavlou et al., 2017, 2018; Scibiorski et 54 al., 2019; Stearns et al., 2015; Storey et al., 2007; Timms et al., 2019). By comparison to zircon, 55 titanite is more reactive and therefore has the potential to display a greater range of petrologic, 56 geochemical, and microstructural variations to inform interpretations of petrogenesis and 57 deformation (Kohn, 2017). The major challenges in applying titanite as a geochronometer are its 58 generally low U and radiogenic Pb concentrations and its tendency to incorporate substantial 59 initial Pb (e.g., Aleinikoff et al., 2002; Frost et al., 2000; Prowatke and Klemme, 2005; Tiepolo 60 61 et al., 2002). Initial Pb (Pb_i) must be corrected for and therefore complicates accurate U-Pb 62 geochronometry of high-Pb_i phases, like titanite, apatite, allanite, and rutile (e.g., Chew et al., 63 64 2014; Kirkland et al., 2017; Rubatto and Scambelluri, 2003; Schoene and Bowring, 2006; Wohlgemuth-Ueberwasser et al., 2017) Here, we use Pb_i to mean the Pb that is incorporated into 65 66 a mineral at the time of crystallization or recrystallization, irrespective of its source and isotopic 67 composition. Pbi includes what is often called "common Pb", Pb representing long-term 68 ingrowth from actinides incorporated in the primordial Earth (Stacey and Kramers, 1975). Pbi 69 can also include Pb acquired from nearby actinide-partitioning minerals that have ingrown Pb 70 with a non-primordial isotopic composition. The most widely used Pbi corrections derive from

the models of Stacey and Kramers (1975) and involve assumptions about Pb_i composition based on the average, reservoir-scale geochemical behavior of Pb – i.e., assumptions about crustal evolution at the scale of an orogenic region, a crustal domain, or even bulk silicate Earth. For Pb_i corrections that employ these models to be accurate, the geochronology sample to which they are applied must be compositionally representative of the large-scale reference reservoir, a requirement that is problematic in the context of intragrain U-Pb measurements. Techniques for *in situ* U-Pb dating, like SIMS/SHRIMP and LA-ICP-MS, complicate Pb_i corrections because they sample micron-scale intracrystalline domains (compositional zones), which may now be chemically and isotopically decoupled from their original environments of formation, including coexisting phase assemblages and fluids. For instance, even when Pb_i is measured in a low-U phase (e.g., K-feldspar) co-located with a zoned geochronometer, it can be difficult to determine which zone within the geochronometer formed in equilibrium with that phase.

A common approach for correcting U-Pb isotope data for Pb_i is to calculate a Pb_i composition based on an estimated age and a crustal evolution model, often the one- or two-stage model of Stacey and Kramers (1975). The two most common variants of this approach are the '204 method' and the '207 method'. In the 204 method, Pb_i ²⁰⁴Pb/²⁰⁶Pb is can be calculated based on a crustal evolution model; measured in a reference material considered representative of the crustal Pb isotope composition for the sample; or measured in a co-existing low-U phase within the sample, such as K-feldspar (DeWolf and Mezger 1994; McGregor et al., 2019), and the total ²⁰⁴Pb/²⁰⁶Pb is measured to determine Pb_i abundance (e.g., Ireland and Williams, 2003; Stern, 1997; Storey et al., 2006; Williams, 1998) (Appendix). In the 207 method, Pb_i ²⁰⁷Pb/²⁰⁶Pb is based on either a model value or a measured value in a co-existing phase, as well as an expected age for the titanite (Appendix). The 204 method has traditionally been preferred for

data collected by SIMS/SHRIMP analysis, during which ²⁰⁴Pb is readily measured (Stern et al., 2009; Stern, 1997; Storey et al., 2006). The 207 method is commonly preferred for data collected by LA-ICP-MS analysis, during which ²⁰⁴Hg contaminants in the Ar plasma interfere on mass 204 (Gehrels et al., 2008; Horstwood et al., 2003; Schoene, 2014; Storey et al., 2006), though recent developments in quadrapole LA-ICP-MS analysis can mitigate this problem. The underpinning assumption for the 204 and 207 method corrections that rely on model values is that the continental crust has evolved as a coherent and largely closed reservoir with respect to U and Pb isotope systematics, and that titanite will crystallize with Pb₁ composition representative of this bulk crustal reservoir. The idea of an "average" or "bulk" composition, however, can break down at the grain scale, where Pb isotope compositions of individual phases depend on phase-specific U and Pb partitioning. For instance, titanite forming from breakdown of rutile may partition radiogenic Pb from rutile in addition to average, ambient Pb, and thus have a different effective Pb_i composition from the bulk rock (Marsh and Smye, 2018). Thus, in situ geochronology of phases that incorporate both U and Pb_i require careful evaluation of Pb_i sources and possible grain-scale U-Pb fractionation.

94

95

96

97

98

99

100

101

102

103

104

105

106

107

108

109

110

111

112

113

114

115

116

Another approach for titanite U-Pb data correction is equivalent to the classic isochron regression method and employs the semi-total Pb/U (Tera-Wasserburg) or total Pb/U diagrams (Ludwig, 1998, 2009, 2012). The samples used to define the linear regression can be permutations of grain separates or individual grains but can also be multiple (e.g., Amelin, 2009; Verts et al., 1996), *in situ* intergrain or intragrain analyses (e.g., Holder and Hacker, 2019; Kohn and Corrie, 2011; Olierook et al., 2018; Storey et al., 2006). In practice, it is common to constrain the Pb_i ²⁰⁷Pb/²⁰⁶Pb composition based on a Stacey and Kramers (1975) model and force the regression through this Pb_i composition (e.g., Kohn and Corrie, 2011). However, it is

becoming more common to treat Pb_i composition as a variable that is retrieved from the regression process (e.g., Kirkland et al., 2017). The Tera-Wasserburg-based isochron regression correction method can avoid the pitfalls of assuming a crustal Pb isotope composition but only works if i) the Pb_i composition is uniform in the grains or domains used to determine the isochron ii) measured grains/domains formed at the same time (are isochronous), and iii) in the case that the Pb_i composition is not fixed a priori, a sufficiently large range of intracrystalline U/Pb and Pb/Pb ratios are sampled to tightly constrain the regression. With recent detailed characterizations of titanite (e.g., Essex and Gromet, 2000; Bonamici et al., 2015; Garber et al., 2017; Marsh and Smye, 2017; Olierook et al., 2018), it is clear that Pb_i can and does vary over timescales of titanite growth and/or recrystallization, undercutting the first requirement for the isochron regression approach in some cases.

U-Pb isotope data for Pb_i-rich phases are treated on the Tera-Wasserburg Concordia diagram in order to explicitly show the Pb_i contribution to U-Pb isotope composition. The Tera-Wasserburg diagram is a two-dimensional projection of the total Pb/U isochron diagram (Ludwig, 1998), which allows for direct display of the Pb_i trends in a dataset. The familiar Wetherill concordia diagram works well for low-Pb_i phases and excels at revealing open system behavior that affects the radiogenic U/Pb ratio (e.g., Schoene, 2014). In contrast, the U-Pb data patterns on the Tera-Wasserburg diagram reflect a combination of Pb_i-radiogenic Pb mixing and open system behavior. Such patterns can, consequently, be less straightforward to interpret.

This work applies different Pb_i correction methods to a suite of well-characterized Grenville-aged titanite grains from the Adirondack Mountains of New York. A review of U-Pb isotope evolution in the semi-total Pb/U isochron (Tera-Wasserburg) diagram illustrates how both intragrain Pb_i compositional variations and grain scale Pb loss can be preserved within *in*

situ data sets. This analytical framework is applied to two U-Pb datasets for the same titanite grains – one collected by SHRIMP and the other collected by LA-ICP-MS. Comparison of the two in situ analytical techniques allows recognition of non-isochronous data and highlights the relative strengths of each technique. These results reinforce both the complexity and opportunities in microanalysis of geochronometers with significant initial Pb.

145

146

147

148

149

150

151

152

153

154

155

156

157

158

159

160

161

140

141

142

143

144

Samples and Methods

Titanite-bearing samples used in this study are high-grade, midcrustal tectonites from the Adirondack region of upstate New York. Titanite grains are hosted in metasyenite collected within the Carthage-Colton mylonite zone, a major structure developed at the boundary between Grenville-aged crustal domains. The Adirondack Lowlands to the northwest of the CCMZ record peak metamorphic conditions during the Shawinigan-AMCG phase of the Grenville orogeny at ca. 1150 Ma, whereas the Adirondack Highlands to the east-southeast of the CCMZ record peak metamorphic conditions during the Ottawan phase at ca. 1050 Ma (Mezger et al., 1993; 1991a; 1991b). The tectonic context of the CCMZ has been previously discussed by Mezger et al. (1991a), Mezger et al. (1991b), Mezger et al. (1992), Mezger et al. (1993), Cartwright et al. (1993), Streepey et al. (2001), Baird and MacDonald (2004), Johnson et al. (2004), Johnson and Selleck (2005), McLelland et al. (2010), and Bonamici et al. (2014). Structural, petrologic, and geochemical characteristics of the specific Harrisville location of samples for the current study have been addressed by Lamb (1993), Cartwright et al. (1993), Baird and MacDonald (2004), Heumann (2004), Johnson and Selleck (2005), Bonamici et al. (2014), and Bonamici et al. (2015).

Regional geochronology provides constraints within which to study and interpret U-Pb titanite data from the CCMZ. Bonamici et al. (2015) documented the intragrain zoning patterns of SHRIMP U-Pb dates within six Harrisville titanite samples (Table 1). Four different generations of titanite were distinguished on the basis of microstructure and reinforced on the basis of chemistry and oxygen-isotope zoning patterns (Bonamici et al., 2014, 2015). These generations are interpreted to be igneous titanite crystallized in the protolith syenite at ~1160 Ma (Type-1); igneous grains variably reset during later granulite-facies metamorphism at ca. 1050 Ma (Type-2); titanite from veins that likely intruded at ca. 1050 Ma (Type-3); and igneous titanite with metamorphic overgrowths (Type-4). Table 1 provides grain descriptions and further information summarizing these interpretations. LA-ICP-MS data presented in this study significantly expand the number of Harrisville titanite grains investigated for U-Pb zoning. U-Pb ratios were measured in a total of fourteen titanite grains, including one Type-1 grain, five Type-2 grains, six Type-3, and two Type-4 grains.

Titanite was analyzed in thin sections of metasyenite cut into one-inch rounds. Thus, all analyzed titanite grains are *in situ* with respect to their host microstructures and phase assemblages. Grains of U-Pb titanite reference material BLR-1 (accepted 206 Pb/ 238 U age 1047 ± 0.4 Ma, Aleinikoff et al., 2007) were embedded in every sample each mount. BLR-1 was used for calibration under the designation BLS at the Arizona Laserchron Center, along with secondary reference material Ecstall West zircon (accepted 206 Pb/ 238 U age $^{91.5}$ ± 1 Ma, Butler et al., 2002), also embedded in each analysis mount. Weighted average ages showing the performance of the reference material grains in each mount during LA-ICP-MS analysis are compiled in the Supplementary Materials. Within $^{2}\sigma$ analytical uncertainties, the dates

determined for these reference materials during SHRIMP and LA-ICP-MS analysis overlap the accepted ages.

184

185

186

187

188

189

190

191

192

193

194

195

196

197

198

199

200

201

202

203

204

205

SIMS U-Pb dates were collected with the SHRIMP II instrument at the Research School of Earth Sciences (RSES) at the Australian National University using a focused, 4.5-nA O₂⁻ primary beam. Data were acquired in single-collector mode with seven successive scans through species ²⁰⁰CaTi₂O₄, ²⁰⁴Pb, ²⁰⁶Pb, ²⁰⁷Pb, ²⁰⁸Pb, ²³⁸U, ²⁴⁸ThO, and ²⁵⁴UO, with each individual analysis taking 20 minutes. SHRIMP analysis sputtered pits 35-40 µm in diameter and 2-3 µm deep (Fig. 1A). Grains of U-Pb titanite standard BLR-1 were analyzed at regular bracketing intervals throughout each analysis session. Total ²³⁸U/²⁰⁶Pb, ²⁰⁷Pb/²⁰⁶Pb, and ²⁰⁴Pb/²⁰⁶Pb ratios reported in Table S1 are corrected for U/Pb instrumental fractionation but are not corrected for Pb_i. SHRIMP radiogenic ratios and ²⁰⁶Pb/²³⁸U dates were initially reported in Bonamici et al (2015), where they were corrected for Pb_i with the 204 method using ²⁰⁴Pb/²⁰⁶Pb measured on long-term RSES lab reference material, Broken Hills feldspar (206Pb/204Pb = 16.00, 207Pb/204Pb = 15.39, and $^{208}\text{Pb}/^{204}\text{Pb} = 35.66$; Gulson, 1984). For the current study, SHRIMP data have been re-corrected (Table S1) with the 204 method using both (1) the Stacey and Kramers (1975) model and (2) the K-feldspar Pb-Pb ratios reported by Mezger et al. (1992) for a shear zone in the Diana metasyentite (sample 90-49: $^{206}Pb/^{204}Pb = 17.132$, $^{207}Pb/^{204}Pb = 15.427$, and 208 Pb/ 204 Pb = 36.461). The dates corrected with Mezger et al. (1992) are preferred because these Pb values come from the same outcrops as the titanite samples used in the current study. To facilitate comparison with LA-ICP-MS data, the SHRIMP data have also been corrected with the 207 method (Table S1) using the Stacey and Kramers (1975) Pb isotope model implemented through the Arizona Laserchron Center spreadsheet software, "Titanite AgeCalc 207Pbc".

Prior to LA-ICP-MS analysis, SHRIMP pits and carbon coats were removed from samples by repolishing with 1-µm diamond-grit suspension. Samples were cleaned with several cycles of sonication in distilled water and ethanol. LA-ICP-MS U-Pb dates were collected on a Nu HR ICP-MS coupled to a Photon Machines Analyte G2 Excimer laser at the Arizona Laserchron Center at the University of Arizona. Data were acquired in static multicollector mode, with ²⁰²Hg and ²⁰⁴Pb collected on ion counters and ²⁰⁶Pb, ²⁰⁷Pb, ²⁰⁸Pb, ²³⁸U, and ²³²Th collected on 10¹¹-ohm resistor Faraday cups. Each analysis included 15 seconds of background counting, 15 one-second laser pulses for sample signal and 30 seconds of wash-out time for a total of approximately 60 seconds per analysis. Laser ablation produced pits 35-40 µm in diameter and ~15 μm deep (Fig. 1B). Grains of U-Pb titanite standard BLR-1 (²⁰⁶Pb/²³⁸U age 1047 Ma, Aleinikoff et al., 2007; also called BLS in the Laserchron lab) were analyzed at regular bracketing intervals throughout each analysis session. Total ²³⁸U/²⁰⁶Pb, ²⁰⁷Pb/²⁰⁶Pb, and ²⁰⁴Pb/²⁰⁶Pb ratios reported in Table S2 were corrected for U/Pb instrumental fractionation, as well as the ²⁰⁴Hg interference on ²⁰⁴Pb. The ²⁰⁴Pb interference correction is accomplished by subtraction of mass 204 counts that are inferred to come from ²⁰⁴Hg based on the measurement of mass 202 and an assumed natural ²⁰²Hg/²⁰⁴Hg ratio of 4.34 (Gehrels et al. 2008). Data in Table S2 and Figures 2, 3, 4, and 6 are not corrected for Pb_i. Radiogenic ratios and ²⁰⁶Pb/²³⁸U dates reported for LA-ICP-MS data (Table S2) were corrected for Pb₁ by an iterative 207 method implemented using internal Arizona Laserchron Center spreadsheet-based software ("Titanite AgeCalc 207Pbc"). This correction uses the raw ²⁰⁶Pb/²³⁸U ratio before Pb_i correction as an initial estimate of expected age and the Stacey and Kramers (1975) model for an estimate of the Pb_i composition (Appendix). The 207-corrected age then recalculated several more times with the 207-corrected age from the previous iteration used as the expected age for each subsequent

206

207

208

209

210

211

212

213

214

215

216

217

218

219

220

221

222

223

224

225

226

227

228

iteration. For titanite U-Pb measurements in this study, the calculation rapidly converges to a stable corrected age within ≤5 iterations. To facilitate comparison with the SHRIMP data, the LA-ICP-MS data have also been corrected with the 204 method (Table S2) using the Stacey and Kramers (1975) model.

Data are compared using total isotope ratios, uncorrected for Pb_i, on Tera-Wasserburg Concordia plots. Error ellipses in Figures 2, 3 and 9 represent 2σ analytical uncertainties, including counting statistics and U/Pb instrumental fractionation (as calibrated with titanite BLR/BLS reference material). Uncertainties on 204 Pb/ 206 Pb for SHRIMP data have been conservatively estimated at 3% (1σ), which is double the largest 207 Pb/ 206 Pb uncertainty reported for SHRIMP data. Uncertainties on all other ratios are as reported by the respective lab (Tables S1 and S2). Error correlations between 238 U/ 206 Pb, 207 Pb/ 206 Pb, and 204 Pb/ 206 Pb ratios are considered to be small and are neglected for the sake of more direct comparison of data arrays.

Two- and three-dimensional linear regressions were implemented in Isoplot 3.75 using Model 1, which weights each measurement by the inverse square of the analytical errors under the assumption that analytical errors are the only source of uncertainty in the data (Ludwig, 2012). A Model 1 regression fit is considered reasonable if the probability of fit is \geq 0.05. Probability of fit for each regression is used as an indicator of additional (geological) sources of scatter. Other models for regression (Models 2 and 3) were not considered to avoid additional assumptions about sources of uncertainty (beyond analytical).

249 Results

When considered in aggregate, LA-ICP-MS and SHRIMP datasets for Harrisville titanite grains define steep, approximately linear trends on Tera-Wasserburg or semi-total Pb/U diagrams

(Fig. 2). The LA-ICP-MS data array spread is larger for two reasons: 1) more than twice as many titanite grains were analyzed by LA-ICP-MS as by SHRIMP (Fig. 3) and many of the grains analyzed by laser had lower Pb_i that extends the array farther toward concordia; and 2) the large ²⁰⁷Pb/²⁰⁶Pb uncertainties on the LA-ICP-MS data for the highest-Pb_i grains appear to stretch the laser data array vertically. However, close comparison of the grains analyzed by both LA-ICP-MS and SHRIMP in Figure 3, shows that, regardless of error ellipse shape, the individual data points are centered at nearly identical locations.

Tera-Wasserburg-based, two-dimensional regression of the aggregate SHRIMP dataset yields a concordia intercept age of 1138 ± 19 Ma with MSWD = 4.4, whereas 2D regression of the aggregate LA-ICP-MS dataset yields a concordia intercept age of 1067 ± 12 Ma with MSWD = 2.0 (Table S3). We note that the regression of SHRIMP data yield a MSWD indicating well scatter beyond that expected based on analytical uncertainty alone, whereas that the precision of LA-ICP-MS data result in a more ambiguous MSWD value. No concordia-intercept ages can be obtained for either aggregate dataset (LA-ICP-MS or SHRIMP) using a total Pb/U isochron (linear 3D) regression that includes the 204 Pb/ 206 Pb ratio (Table 1).

For Harrisville titanite samples, greater 238 U/ 206 Pb (average 2.3% 1 \sigma) than 207 Pb/ 206 Pb analytical uncertainties (average 1.0% 1 \sigma) suggest that the U/Pb calibration dominates overall SHRIMP analytical uncertainties. In contrast, greater 207 Pb/ 206 Pb (average 5.1% 1 \sigma) than 238 U/ 206 Pb (average 2.6% 1 \sigma) analytical uncertainties indicate that abundance sensitivity dominates overall LA-ICP-MS analytical uncertainties.

On a grain-by-grain basis, both SHRIMP and LA-ICP-MS U-Pb measurements show a range of behavior, with several grains having tightly clustered data (i.e. showing limited ²³⁸U/²⁰⁶Pb or ²⁰⁷Pb/²⁰⁶Pb dispersion) (Fig. 3). For those grains with tightly clustered spot

analyses, both 2D and 3D regressions of the U-Pb measurements yield large concordia-intercept age uncertainties (> ±50 Ma), as well as large MSWD values for SHRIMP data sets. Titanite grains from sample HA13 are an exception, showing sufficient analysis dispersion to provide moderately tight constraints on concordia-intercept ages regressed from LA-ICP-MS data (Fig. 3). SHRIMP U-Pb measurements for the HA13 S2 grain show a similar dispersion to LA-ICP-MS measurements and similar concordia-intercept age but with high MSWD values.

Results from 3D linear isochron regressions for each titanite Type are described below with respect to the concordia-intercept age and the regressed Pbi ²⁰⁷Pb/²⁰⁶Pb value (Table 1, Fig. 4). Several unconstrained 3D regressions produce negative ²⁰⁷Pb/²⁰⁶Pb (y-axis) intercept values because tightly clustered data do not adequately constrain the linear regression toward the common Pb plane, resulting in a very large range of possible intercept values with a negative mean. Several constrained 3D regressions produce undefined ²⁰⁷Pb/²⁰⁶Pb values because very large uncertainties push the mean regressed ²⁰⁶Pb/²⁰⁴Pb value to zero (Table 1), the lowest allowed ²⁰⁶Pb/²⁰⁴Pb value for a constrained regression solution. Table S3 shows 2D regression results, but these are not discussed in the text in order to avoid redundancy and because the larger uncertainties on the 2D regression results generally hide details within the datasets.

Type 1 titanite results

Constrained 3D linear concordia intercept dates for the Type-1 grain for both LA-ICP-MS and SHRIMP data are > 1200 Ma, with large uncertainties of > 200 m.y. (Table 1). The unconstrained regression of LA-ICP-MS data intercepts concordia within analytical uncertainties, but the unconstrained regression of more precise SHRIMP data set does not (Fig 4B). The Type-1 titanite grain has both the highest and largest range of ²⁰⁴Pb/²⁰⁶Pb ratios (Tables S1 and S2). The Type-1 grain also has the lowest overall U, Th, and Pb concentrations. LA-ICP-

MS data points from this low-Pb grain all overlap significantly within error and no interpretable ²⁰⁷Pb/²⁰⁶Pb intercept is obtained with either constrained or unconstrained 3D regressions (Table 1). An unconstrained regression of the more precise SHRIMP data yields an upper intercept ²⁰⁷Pb/²⁰⁶Pb value of 0.967, similar to the Stacy and Kramers common Pb value of 0.922, though with large uncertainties (Table 1).

Type 2 titanite results

Type-2 titanite grains yield tightly clustered U-Pb data points, both within individual grains (Fig. 3) and between grains (Fig. 2). Constrained 3D linear regressions of LA-ICP-MS data return concordia-intercept ages of 1143-1111 Ma, whereas regressions of SHRIMP data return consistently older concordia-intercept ages of 1182-1146 Ma (Table 1). Both methods produce intercept-age uncertainties of 48-130 m.y., and the SHRIMP data regressions are also associated with large MSWD values. Both constrained and unconstrained regressions yield largely uninterpretable ²⁰⁷Pb/²⁰⁶Pb upper intercept values (Table 1), with the possible exception of grain HA09A S15, which gives values consistent with a mixture of primordial (Stacey and Kramers common Pb) and radiogenic Pb_i.

Type 3 titanite results

Aggregated Type-3 data show greater dispersion than Type-2 data, but data for individual Type-3 grains are more clustered than the aggregate dataset (Fig. 3). Constrained 3D isochron regressions of LA-ICP-MS Type-3 data yield the youngest concordia intercept ages, ranging from 935 Ma to 1101 Ma (Table 1, Fig. 4). Some of the older LA-ICP-MS dates have moderate analytical uncertainties of 28-38 m.y., but many LA-ICP-MS dates are associated with large analytical uncertainties of 63-190 m.y.. Constrained 3D regression for the one SHRIMP-analyzed Type-3 grain produces an imprecise concordia intercept age of 1220 ± 370 Ma.

Constrained and unconstrained regressions for most LA-ICP-MS-analyzed grains produce ²⁰⁷Pb/²⁰⁶Pb upper intercepts intermediate between the expected radiogenic value (~0.08) and the expected Stacey and Kramers common-Pb model value (~0.92), though often with very large uncertainties.

Type 4 titanite results

Data from the Type-4 grains, in aggregate and individually, define approximately linear or apparently offset linear trends. Whereas overlap in LA-ICP-MS data for grain HA13A-S1 obscures distinct internal data populations, three data populations can be distinguished in both the LA-ICP-MS and SHRIMP data for HA13A-S2 (Fig. 3). Constrained and unconstrained regressions of both LA-ICP-MS and SHRIMP data produce very similar Tera-Wasserburg plane intercepts and concordia intercept ages at 1124-1128 Ma (Table 1, Fig. 4). Uncertainties on LA-ICP-MS data are ~25 m.y. and those for the SHRIMP data are three times larger at 75 m.y.. In addition, the MSWD value for the regression of the SHRIMP data is much larger than the MSWD value for LA-ICP-MS data. Most constrained and unconstrained regressions for both analytical techniques produce ²⁰⁷Pb/²⁰⁶Pb upper intercepts intermediate between the expected radiogenic value (~0.08) and the expected Stacy and Kramers common Pb model value (~0.92). The constrained regression for the SHRIMP-analyzed grain produces a ²⁰⁷Pb/²⁰⁶Pb upper intercept greater than the expected Stacy and Kramers common Pb model value, though with large uncertainties.

Zoning trends within titanite grains

In situ U-Pb data can also be assessed in the context of their spatial distribution within titanite grains (Fig 5; Supplemental Figures; Bonamici et al., 2015). The lower precision of LA-ICP-MS measurements precludes definitive recognition of intragrain zoning as the oldest and

youngest Pbi-correct dates determined for any given grain overlap within 2σ uncertainties; however, similarity of intragrain trends in grains for which both more precise SHRIMP data and LA-ICP-MS data exist (Fig. 5), suggests that the LA-ICP-MS data are indicative of zoning. Generally, both LA-ICP-MS and SHRIMP yield older ²⁰⁶Pb/²³⁸U dates toward grain centers and younger dates near grain edges (Fig 5; Supplemental Figures); however, there is considerable intragrain variability in Pbi-corrected dates (particularly for SHRIMP data), which range from pre-Shawinigan (>1180 Ma) to post-Ottawan (975 Ma). This result is the same, whether the Pbi model is the traditional Stacey and Kramers (1975), the ANU lab Broken Hill feldspar, or the Mezger et al. (1992), providing that the same Pbi composition is used for all corrections (Table S1). For a given grain, most Pbi-corrected dates differ significantly from the mean constrained concordia-intercept date (Fig 5; Supplemental Figures); however, almost all dates overlap within large uncertainties associated with both the individual Pbi date corrections and the isochron regressions.

358 Discussion

Comparison of LA-ICP-MS and SHRIMP analysis of titanite

The collection and comparison of parallel U-Pb data sets for Harrisville titanite allows us to examine the tradeoffs in analytical precision and data collection rates between the two techniques for these grains. In general, both techniques recover very similar ranges in isotope ratios, but the higher analytical precision of the SHRIMP data resolves intragrain complexity that is obscured by the lower analytical precision of the LA-ICP-MS data. Consequently, the precision of dates determined through individual Pb_i correction is generally lower for LA-ICP-MS than for SHRIMP (Fig. 5; Tables S1 and S2), reflecting larger uncertainties in the Pb isotope

measurements by LA-ICP-MS and their propagation through the 207-method correction. On the other hand, the precision of concordia intercepts is generally poorer for SHRIMP than for LA-ICP-MS (Fig. 4), reflecting greater resolvable geologic scatter in the more precise SHRIMP data and thus poorer fits for linear regressions.

367

368

369

370

371

372

373

374

375

376

377

378

379

380

381

382

383

384

385

386

387

388

389

In situ U-Pb data collected within titanite grains are commonly assumed to represent single age and Pb_i populations and are treated as such through the isochron regression method. The facts that the aggregated Harrisville data (1) cannot be fit with a 3D regression and (2) yield dates ~70 m.y. apart for 2D regressions (Table 2) point toward significant grain-to-grain age and/or Pbi heterogeneity. Dates determined by the isochron regression method for within-grain U-Pb data generally overlap the time period spanning the two known orogenic events in the Adirondack Mountains, from beginning of the AMCG-Shawinigan phase at ca. 1180 Ma through the end of the Ottawan phase at ca. 1010 Ma (Fig. 4). The poor precision on these regression dates, however, rarely allows a given date to be clearly assigned to one orogenic phase or the other, let alone to a restricted period within one of the orogenic phases (Figs. 3, 4). The spread of regression-determined dates is consistent with the conclusion from previous work that the Harrisville titanite grains record both the AMCG-Shawinigan and Ottawan events (Bonamici et al., 2015). It also suggests that regressions are not true isochrons, but rather that they are fits to mixed, non-isochronous data that are variably resolved with different in situ measurement techniques (see below for further discussion). Larger analytical uncertainties for LA-ICP-MS data, especially, mask the probable geologic scatter within the data, producing isochron regressions with MSWD values ≤ 1 and probabilities of fit > 0.05. Only relatively large propagated uncertainties, typically $\geq \pm 50$ m.y., suggest the presence of geologic scatter within the LA-ICP-MS datasets. By comparison, geologic scatter is more apparent in regressions of

SHRIMP data for the same titanite grains, which produce large MSWD values, probabilities of fit close to zero, and large propagated uncertainties (Fig. 3).

390

391

392

393

394

395

396

397

398

399

400

401

402

403

404

405

406

407

408

409

410

411

412

Regression-determined dates and Pbi-corrected dates for a given grain can be compared to check for internal consistency between the analytical and correction methods. An ideal titanite grain that has crystallized at a single time, though with a range of Pbi concentrations, should produce Pb_i-corrected dates that are identical to one another and to the regressed concordiaintercept date. Differences in Pbi-corrected dates and/or discrepancy between Pbi-corrected and regression-determined concordia-intercept dates would suggest internal zoning and nonisochronous grain crystallization. Pbi-corrected dates are, in fact, not identical across Adirondack titanite grains. Intragrain zoning of Pbi-corrected dates is statistically resolvable along most traverses measured by SHRIMP, though not by LA-ICP-MS (Fig. 5); nonetheless, the similarity between several SHRIMP and LA-ICP-MS profile shapes suggests that LA-ICP-MS is detecting similar isotopic variability. Similarly, Pbi-corrected dates and regressed concordia-intercept dates for a given grain generally overlap within the propagated uncertainties of the respective correction methods (Fig. 5). However, the resolvable intragrain zoning of Pb_i-corrected SHRIMP dates and the poor fit metrics for many of the concordia-intercept regressions suggest that this overlap is an artefact of temporally close events (≤100 m.y. apart at greater than 1 Ga) and relatively large analytical uncertainties on the *in situ* data.

The LA-ICP-MS and SHRIMP datasets for several Adirondack titanite grains also allow for assessment of differential Pb isotope sensitivity and its potential effects on the accuracy of Pb_i-corrected dates. Specifically, differential sensitivity to higher-abundance ²⁰⁶Pb relative to lower-abundance ²⁰⁴Pb or ²⁰⁷Pb could skew measured Pb/Pb ratios used for Pb_i corrections. A quick check for differential Pb isotope sensitivity is to compare 204-corrected versus 207-

corrected dates for both the SHRIMP and LAICPMS datasets. SHRIMP data corrected with the 204 and 207 methods yield dates that are essentially identical (Table S1), suggesting that SHRIMP Pb/Pb ratios are not skewed by differential Pb isotope sensitivity. LA-ICP-MS data corrected by the 204 and 207 methods yield different dates, with those corrected by the 204 method always systematically younger (Table S2). Differences between the LA-ICP-MS and SHRIMP datasets can be compared graphically by plotting total ²⁰⁷Pb/²⁰⁶Pb vs. total ²⁰⁴Pb/²⁰⁶Pb covariation trends (Fig. 6). The slopes of the covariation trends are markedly different, with the steeper slope for the LA-ICP-MS data arising from the systematically lower ²⁰⁴Pb/²⁰⁶Pb values and indicating lower ²⁰⁴Pb sensitivity relative to SHRIMP. On the other hand, the similar range of ²⁰⁷Pb/²⁰⁶Pb measured by LA-ICP-MS and SHRIMP indicates that LA-ICP-MS-determined ²⁰⁷Pb/²⁰⁶Pb ratios are unaffected by differential Pb isotope sensitivity in these samples. Note that for the purposes of this discussion, the term Pb sensitivity includes the effects of instrument sensitivity, the ²⁰⁴Hg interference correction applied to LA-ICP-MS-measured ratios, and downhole Pb isotope fractionation. Because LA-ICP-MS ²⁰⁴Pb/²⁰⁶Pb ratios but not ²⁰⁷Pb/²⁰⁶Pb ratios are affected, correction for ²⁰⁴Hg, which affects only the ²⁰⁴Pb/²⁰⁶Pb ratio, seems a likely culprit for creating a differential Pb isotope sensitivity problem. This comparison suggests cautious application of ²⁰⁴Hg corrections to LA-ICP-MS data for high Pb_i phases and use of the 207 method if differential Pb isotope sensitivity is suspected.

431

432

433

434

435

413

414

415

416

417

418

419

420

421

422

423

424

425

426

427

428

429

430

U-Pb isochron evolution on the Tera-Wasserburg (semi-total Pb/U) diagram

Ideally, when a set of titanite grains or domains crystallizes at the same time, the U-Pb data for this population will define sloped linear arrays in Tera-Wasserburg space. Such arrays are often referred to as discordia by analogy with the familiar Wetherill-diagram zircon

discordia, which form as a result of changes to the U/Pb ratio due to open-system U or Pb loss. In titanite with no Pb_i, open-system modification of the U/Pb ratio would also produce a sloped, discordant array of data (Tera and Wasserburg 1974; Schoene 2014). However, most titanite incorporates Pb_i, and sloped, linear arrays are more often mixing arrays treated as isochrons resulting from variable U/Pb_i ratio (μ). If the data are precise and well-spaced (have a range of U/Pb_i), then a regression provides a tightly constrained upper y-axis intercept at the shared Pb_i 207 Pb/ 206 Pb value and lower intercept with the Tera-Wasserburg concordia at the age of crystallization.

The Tera-Wasserburg concordia is the locus of the time-integrated ²⁰⁷Pb/²⁰⁶Pb and ²³⁸U/²⁰⁶Pb ratios resulting from U decay in the absence of Pb_i; each point along the concordia is an implicit function of initial ²³⁵U/²³⁸U, and thus time of crystallization. Paths in Figure 7A show the temporal evolution of radiogenic ²⁰⁷Pb/²⁰⁶Pb and ²³⁸U/²⁰⁶Pb ratios for several initial ²³⁵U/²³⁸U ratios. For titanite crystallized since ~3.0 Ga, the temporal evolution paths are nearly parallel to the ²³⁸U/²⁰⁶Pb axis because of the much greater relative change in ²³⁸U/²⁰⁶Pb as compared to ²⁰⁷Pb/²⁰⁶Pb during radiogenic Pb ingrowth.

The addition of Pb_i to titanite constrains the starting points of the temporal evolution paths to a fixed ²⁰⁷Pb/²⁰⁶Pb value (Fig. 7B). The shapes of the evolution paths depend on the evolving relative proportions of Pb_i with a fixed ²⁰⁷Pb/²⁰⁶Pb composition and radiogenic Pb, growing in with a time-varying ²⁰⁷Pb/²⁰⁶Pb composition (Fig. 7B, pale gray curves). For proportionally higher Pb_i, evolution paths are steeper, reflecting the dominance of the fixed ²⁰⁷Pb/²⁰⁶Pb value of the Pb_i. For lower Pb_i, evolution paths are shallower, reflecting dominance of the time-varying radiogenic ²⁰⁷Pb/²⁰⁶Pb ratio. Titanite domains that crystallize at the same time and have remained closed throughout their evolution but contain varying concentrations of

Pb_i will defined a mixing line between the Pb_i composition and the radiogenic Pb composition at any given time. This mixing line will evolve in a systematic way with time, sweeping toward lower ²⁰⁷Pb/²⁰⁶Pb and ²³⁸U/²⁰⁶Pb, and is thus an isochron (Fig. 7B, dark gray lines). When the Pb_i composition incorporated into titanite has a lower ²⁰⁷Pb/²⁰⁶Pb, the initial Pb-radiogenic Pb mixing line and the resulting isochrons will have shallower slopes (Fig. 7C, blue lines). Consequently, linear arrays of titanite U-Pb data that show changes in slope (curve or bend) or appear to intersect with other linear arrays are indicative of changes in Pb_i composition during crystallization or recrystallization.

Fractionation of U and Pb results in titanite with variable U/Pb ratio and can arise from differential mobility of these elements during crystallization, recrystallization or intragrain diffusion. In titanite that also incorporates Pb_i, fractionation of U and Pb manifests as subhorizontal data arrays that approximately parallel the ²³⁸U/²⁰⁶Pb axis on the Terra-Wasserburg diagram (Fig. 7D, E). Changes in U/Pb ratio that occur long after initial titanite crystallization should generate more horizontal arrays than changes to U/Pb ratios that occur shortly after crystallization (Fig. 7E; Tera and Wasserburg, 1974) because Pb_i makes ups a larger proportion of total Pb in titanite early on. Pb loss can occur by Pb diffusion or by recrystallization that produces a higher U/Pb ratio than present in earlier-formed titanite. Significant U diffusion in titanite is unlikely (Frost et al., 2000); however, real or apparent U loss can occur when recrystallization produces a lower U/Pb ratio than present in earlier-formed titanite. Significant U loss can produce reverse discordance on the Tera-Wasserburg diagram (Fig. 7D).

Pb isotopic fractionation during diffusion is expected to be negligible because of the small relative mass differences between Pb isotopes. Pb isotopic variations during recrystallization will also be negligible in the case that earlier-formed titanite is the primary

source of Pb to later-formed titanite (e.g., interface coupled dissolution-precipitation recrystallization of Holder and Hacker (2019)). Significant changes to both the U/Pb and Pb/Pb ratios of titanite are anticipated when recrystallization occurs in the presence of fluids that are not in equilibrium with respect to the titanite-stabilizing phase assemblage – i.e. fluids external to the local rock system.

487

488

489

490

491

492

493

494

495

496

497

498

499

500

501

502

503

482

483

484

485

486

Interpretation of the Harrisville titanite data from Tera-Wasserburg data patterns

The curvature in Adirondack titanite U-Pb data arrays suggest variation in Pbi composition. Both LA-ICP-MS and SHRIMP data show an approximately linear trend with a slight curvature toward lower slope at ²⁰⁷Pb/²⁰⁶Pb ~0.12 (Fig. 2). This is expressed by a small offset of some Type-3 and Type-4 data relative to Type-1 and Type-2 data, as well as by greater dispersion of data within Type-3 and Type-4 grains relative to Type-2 grains (Fig. 3). Departure from a single linear isochron is also supported by the lack of a three-dimensional model solution for the aggregate data sets (Table 1). The curvature of the Adirondack data arrays suggests that titanite incorporated at least two different compositions of Pbi, as do linear regressions that project toward varied Pb_i ²⁰⁷Pb/²⁰⁶Pb values, some of which are significantly lower than ~0.92 (Table 1). The subtlety of the array curvature makes defining linear segments by eye and dividing the data into Pb_i compositional groups challenging and potentially quite arbitrary. Differences in Pb_i composition can arise from variations in growth or recrystallization environment (Bonamici et al., 2015; Kohn, 2017; Lucassen et al., 2011; Marsh and Smye, 2017; Romer and Rötzler, 2003; Scibiorski et al., 2019), which should also be reflected in other compositional proxies, such as REE content, δ^{18} O, or Th/U ratio. Thus, additional compositional information might be used to identify and define data populations that can appropriately be regressed together.

In addition to multiple Pb_i components, titanite U-Pb data also show evidence for Pb loss. For a given ²⁰⁷Pb/²⁰⁶Pb ratio, U-Pb data are dispersed subparallel to the ²³⁸U/²⁰⁶Pb axis (Fig. 8). The ²⁰⁴Pb/²⁰⁶Pb ratio decreases toward the concordia (Fig. 8A), but for a given ²⁰⁴Pb/²⁰⁶Pb value, the ²⁰⁴Pb-corrected dates decrease systematically parallel to the ²³⁸U/²⁰⁶Pb axis (Fig. 8B). This subhorizontal date gradient is consistent with Pb loss altering the ²³⁸U/²⁰⁶Pb ratio (Fig. 7D, E). Diffusive Pb loss has been suggested for these grains based on previous work demonstrating diffusion of oxygen isotopes, which have similar diffusivity to Pb at granulite facies conditions (Cherniak, 1993; Zhang et al., 2006), and a lack of correlation between chemical and isotopic zoning in the Harrisville grains (Bonamici et al., 2014; 2015).

A quantitative model of Pb ingrowth and Pb loss can be constructed to approximate the Harrisville titanite history (Fig. 9; Supplemental Materials). It shows that significant Pb loss ~100 m.y. after initial titanite crystallization produces data scatter that is consistent with both the direction and magnitude of offset of Harrisville U-Pb data relative to a 1150-Ma isochron (cf. Fig. 8). The model predicts that more recent Pb loss would have shifted the U-Pb data toward significantly higher ²³⁸U/²⁰⁶Pb than observed. Thus, the relatively small, subhorizontal dispersion of U-Pb data on the Tera-Wasserburg diagram is consistent with magmatic titanite crystallization at ca. 1160 Ma followed by Pb loss during granulite-facies metamorphism at ca.1050 Ma.

Implications for interpreting (in situ) U-Pb titanite data

Generalizing the geometric considerations of the Tera-Wasserburg diagram and the results from the Harrisville titanite example, U-Pb data patterns can be used to recognize both

Pb_i compositional variations on the grain scale and open-system U/Pb fractionation. Previous workers have long understood that data that form sloped linear arrays indicate a shared Pb_i composition and isochronous formation (Ludwig, 1998; Storey et al., 2006; Tera and Wasserburg, 1972; 1974). Indeed, these types of datasets were the motivation for the development of the Tera-Wasserburg diagram. In many cases, linear data arrays can be appropriately regressed to find both the shared, single crystallization age and Pb_i composition (e.g., Stearns et al., 2016; Marsh and Smye, 2017).

In contrast, intersecting and/or curved arrays (e.g., Kirkland et al., 2016) suggest non-isochronous (re)crystallization and variations in the Pbi composition. Ideally, if distinct linear segments can be recognized within a curved array, the subset of data defining a given segment can be regressed to find an isochron. This analysis also suggests that curved arrays with progressively shallower slopes toward the right, toward higher U/Pb, on the Tera-Wasserburg diagram, are expected because ingrowth of radiogenic Pb over time potentially supplies an increasing radiogenic component to the Pbi being incorporated into newly (re)crystallized titanite.

Data arrays that are dispersed parallel to the ²³⁸U/²⁰⁶Pb axis (e.g., Scibiorski et al., 2019) suggest open-system alteration of the U/Pb ratio in an existing titanite grain by diffusion or (re)crystallization, possibly in the presence of a variable-composition fluid. In general, horizontally dispersed data should be treated with caution in choosing isochron regressions because data may have been shifted toward either lower or higher ²³⁸U/²⁰⁶Pb by open-system U/Pb fractionation. Depending on the length scale of U or Pb mobility, ²³⁸U/²⁰⁶Pb may be shifted to both higher *and* lower values within the same grain (i.e., dispersed horizontally away from the central, true isochron location). Bidirectional dispersal would be expected in the case that Pb

diffusion depletes Pb from some regions of a grain while enriching other regions. Our results also suggest that reversely discordant points (data that fall to the left of the Tera-Wasserburg concordia) have been shifted subparallel to the ²³⁸U/²⁰⁶Pb axis as a result of open-system recrystallization that decreases the U/Pb ratio.

In some cases, a subset of titanite U-Pb data form a linear array that can be regressed with the isochron method whereas other data fall significantly off the linear array (e.g., Garber et al. 2017). Analyses that do not form part of the linear isochron array represent titanite domains that, relative to the data the define the linear isochron array, have incorporated a different Pbi composition, (re)crystallized at a different time, or a combination of both. These patterns cannot be created by simple variations in the relative proportions of the same Pbi and radiogenic Pb between analyses.

Finally, data that form a cloud above concordia without well defined, linear or curvilinear, sloped or horizontal, arrays (e.g., Kohn and Corrie, 2011; Garber et al., 2017) reflect some combination of U/Pb fractionation, changing Pb_i composition, and/or variable crystallization age during titanite formation. Interpretation of age significance from such datasets requires additional geologic, petrologic, and microstructural constraints and/or a prior knowledge of expected age populations.

568 Implications

Titanite is an opportunistic mineral with highly adaptive crystal chemistry (e.g., Frost et al., 2001; Kohn, 2017), and, as yet, the connections between titanite trace element content and titanite (re)crystallization environment remain only partially explored, especially in subsolidus hydrothermally altered and/or metamorphic titanite. Multiple processes can apparently produce

similar trace element variations and patterns in titanite. For instance, microscale intragrain variations in high field strength elements have been linked to fine-scale fluid composition variations (Lucassen et al., 2010a; 2010b; 2011; Gao et al., 2012; Chen et al., 2016), sector zoning and trace element entrapment during growth (Hayden et al., 2008; Kohn, 2017), and equilibrium or disequilibrium dissolution-reprecipitation processes (Romer and Rötzler, 2003; Olierook et al., 2018; Hartnady et al., 2019; Holder and Hacker, 2019). Trends in titanite rare earth element and actinide contents have also been linked to dissolution-reprecipitation (Garber et al., 2017), as well as to coeval allanite or garnet growth (Garber et al., 2017; Scibiorski et al., 2019), and sector zoning (Kohn, 2017; Bruand et al., 2019). Collectively, these studies suggest that titanite chemistry can record equilibrium trace-element partitioning, especially between titanite and melt, but that equilibrium may be very local (at the scale of grains) and/or that titanite can reflect kinetic limitations on element mobility, attachment, or detachment. Approaches like the Tera-Wasserburg analysis utilized in this study help to reduce the effect of these poorly understood controls on the interpretation of U-Pb systematics by allowing Pbi variations to be distinguished from U/Pb ratio variations, regardless of the exact process(es) responsible.

573

574

575

576

577

578

579

580

581

582

583

584

585

586

587

588

589

590

591

592

593

594

Moreover, when combined with grain-scale characterization of element and isotopic zoning, the Tera-Wasserburg-based analysis of this study demonstrates an approach for maximizing geochronologic information obtained by *in situ* U-Pb titanite analysis, especially for rocks with polyphase thermal histories. The approach described here also aids in identifying sources of uncertainty in U-Pb data, whether arising from the analysis itself or from actual geological variability. Even when precise dates are not recovered, geological processes and

events that cause data scatter can be recognized through analysis of U-Pb data patterns using the Tera-Wasserburg diagram.

Acknowledgements

We thank C. Mark Fanning of the Research School of Earth Sciences at the Australian National University for enabling SHRIMP U-Th-Pb data collection. We thank Nicki Geisler and Mark Pecha of the Arizona Laserchron Center for supporting LA-ICP-MS U-Th-Pb analysis and providing data analysis spreadsheets. Brian Hess expertly prepared samples. This work was supported through the National Science Foundation [grant number EAR-0838058] (award to John Valley). We also thank two anonymous reviewers for useful comments and suggestions for the improvement of this manuscript.

606	References Cited
607	Aleinikoff, J.N., Wintsch, R.P., Fanning, C.M., and Dorais, M.J. (2002) U-Pb geochronology of
608	zircon and polygenetic titanite from the Glastonbury Complex, Connecticut, USA: an
609	integrated SEM, EMPA, TIMS, and SHRIMP study. Chemical Geology, 188, 125-147.
610	Aleinikoff, J.N., Horton, J.W., Drake, A.A., Wintsch, R.P., Fanning, C.M., and Yi, K. (2004)
611	Deciphering multiple Mesoproterozoic and Paleozoic events recorded in zircon and
612	titanite from the Baltimore Gneiss, Maryland: SEM imaging, SHRIMP U-Pb
613	geochronology, and EMP analysis. In Proterozoic Tectonic Evolution of the Grenville
614	Orogen in North America Vol. 197, pp. 411-434. Geological Society of America.
615	Aleinikoff, J.N., Wintsch, R.P., Tollo, R.P., Unruh, D.M., Fanning, C.M., and Schmitz, M.D.
616	(2007) Ages and origins of rocks of the Killingworth dome, south-central Connecticut:
617	Implications for the tectonic evolution of southern New England. American Journal of
618	Science, 307, 63–118.
619	Amelin, Y. (2009) Sm-Nd and U-Pb systematics of single titanite grains. Chemical Geology,
620	261, 53–61.
621	Baird, G.B., and MacDonald, W.D. (2004) Deformation of the Diana syenite and Carthage-
622	Colton mylonite zone: Implications for timing of Adirondack Lowlands deformation. In
623	Memoir 197: Proterozoic Tectonic Evolution of the Grenville Orogen in North America
624	Vol. 197, pp. 285–297. Geological Society of America.
625	Bonamici, C.E., Kozdon, R., Ushikubo, T., and Valley, J.W. (2014) Intragrain oxygen isotope
626	zoning in titanite by SIMS: Cooling rates and fluid infiltration along the Carthage-Colton
627	Mylonite Zone, Adirondack Mountains, NY, USA. Journal of Metamorphic Geology, 32,
628	71–92.

629	Bonamici, C.E., Fanning, C.M., Kozdon, R., Fournelle, J.H., and Valley, J.W. (2015) Combined
630	oxygen-isotope and U-Pb zoning studies of titanite: New criteria for age preservation.
631	Chemical Geology, 398, 70–84.
632	Butler, R.F., Gehrels, G.E., Baldwin, S.L., and Davidson, C. (2002) Paleomagnetism and
633	geochronology of the Ecstall pluton in the Coast Mountains of British Columbia: Evidence
634	for local deformation rather than large-scale transport. Journal of Geophysical Research:
635	Solid Earth, 107, EPM 3-1.
636	Bruand, E., Storey, C., Fowler, M., and Heilimo, E. (2019) Oxygen isotopes in titanite and
637	apatite, and their potential for crustal evolution research. Geochimica et Cosmochimica
638	Acta, 255, 144–162.
639	Cartwright, I., Valley, J., and Hazelwood, AM. (1993) Resetting of oxybarometers and oxygen
640	isotope ratios in granulite facies orthogneisses during cooling and shearing, Adirondack
641	Mountains, New York. Contributions to Mineralogy and Petrology, 113, 208-225.
642	Chen, YX., Zhou, K., Zheng, YF., Gao, XY., and Yang, Y.H. (2016) Polygenetic titanite
643	records the composition of metamorphic fluids during the exhumation of ultrahigh-
644	pressure metagranite in the Sulu orogen. Journal of Metamorphic Geology, 34, 573-594.
645	Cherniak, D.J. (1993) Lead diffusion in titanite and preliminary results on the effects of radiation
646	damage on Pb transport. Chemical Geology, 110, 177-194.
647	——— (2010) Diffusion in Accessory Minerals: Zircon, Titanite, Apatite, Monazite and
648	Xenotime. Reviews in Mineralogy and Geochemistry, 72, 827–869.
649	Chew, D.M., Petrus, J.A., and Kamber, B.S. (2014) U-Pb LA-ICPMS dating using accessory
650	mineral standards with variable common Pb. Chemical Geology, 363, 185–199.

DeWolf, C.P., and Mezger, K. (1994) Lead isotope analyses of leached feldspars: Constraints on 651 the early crustal history of the Grenville Orogen. Geochimica et Cosmochimica Acta, 58, 652 653 5537–5550. Essex, R.M., and Gromet, L.P. (2000) U-Pb dating of prograde and retrograde titanite growth 654 during the Scandian orogeny. Geology, 28, 419–422. 655 656 Frost, B.R., Chamberlain, K.R., and Schumacher, J.C. (2001) Sphene (titanite): phase relations and role as a geochronometer. Chemical Geology, 172, 131–148. 657 Gao, X.-Y., Zheng, Y.-F., Chen, Y.-X., and Guo, J. (2012) Geochemical and U-Pb age 658 constraints on the occurrence of polygenetic titanites in UHP metagranite in the Dabie 659 orogen. Lithos, 136–139, 93–108. 660 Garber, J.M., Hacker, B.R., Kylander-Clark, A.R.C., Stearns, M., and Seward, G. (2017) 661 Controls on Trace Element Uptake in Metamorphic Titanite: Implications for 662 Petrochronology. Journal of Petrology, 58, 1031–1057. 663 664 Gehrels, G.E., Valencia, V.A., and Ruiz, J. (2008) Enhanced precision, accuracy, efficiency, and spatial resolution of U-Pb ages by laser ablation-multicollector-inductively coupled 665 plasma–mass spectrometry. Geochemistry, Geophysics, Geosystems, 9. 666 667 Gulson, B.L. (1984) Uranium-lead and lead-lead investigations of minerals from the Broken Hill 668 lodes and mine sequence rocks. Economic Geology, 79, 476–490. 669 Hartnady, M.I.H., Kirkland, C.L., Clark, C., Spaggiari, C.V., Smithies, R.H., Evans, N.J., and 670 671 McDonald, B.J. (2019) Titanite dates crystallisation; slow Pb diffusion during supersolidus re-equilibration. Journal of Metamorphic Geology, 37, 823–838. 672 Heumann, Mattew J. (2004) Thermochronological and Geochronological studies in the 673 Adirondack Highlands and Lowlands, New York. Syracuse University. 674

Holder, R.M., and Hacker, B.R. (2019) Fluid-driven resetting of titanite following ultrahigh-675 temperature metamorphism in southern Madagascar. Chemical Geology, 504, 38–52. 676 Horstwood, M.S., L. Foster, G., R. Parrish, R., R. Noble, S., and M. Nowell, G. (2003) 677 Common-Pb corrected in situ U-Pb accessory mineral geochronology by LA-MC-ICP-678 MS. Journal of Analytical Atomic Spectrometry, 18, 837–846. 679 680 Ireland, T.R., and Williams, I.S. (2003) Considerations in Zircon Geochronology by SIMS. Reviews in Mineralogy and Geochemistry, 53, 215–242. 681 Johnson, E.L., Goergen, E.T., and Fruchey, B.L. (2004) Right lateral oblique slip movements 682 followed by post-Ottawan (1050–1020 Ma) orogenic collapse along the Carthage-Colton 683 shear zone: Data from the Dana Hill metagabbro body, Adirondack Mountains, New 684 York. In Memoir 197: Proterozoic Tectonic Evolution of the Grenville Orogen in North 685 America Vol. 197, pp. 357–378. Geological Society of America. 686 Johnson, E.L., Selleck, B.W., DeLorraine, B., and Lupulescu, M. (2005) The nature and 687 688 significance of the Carthage-Colton shear zone and related late-to-post tectonic granites and ore deposits. Friends of the Grenville. 689 Jung, S., and Hellebrand, E. (2007) Textural, geochronological and chemical constraints from 690 691 polygenetic titanite and monogenetic apatite from a mid-crustal shear zone: An integrated EPMA, SIMS, and TIMS study. Chemical Geology, 241, 88–107. 692 693 Kirkland, C.L., Spaggiari, C.V., Johnson, T.E., Smithies, R.H., Danišík, M., Evans, N., Wingate, 694 M.T.D., Clark, C., Spencer, C., Mikucki, E., and others (2016) Grain size matters: 695 Implications for element and isotopic mobility in titanite. Precambrian Research, 278, 283-302. 696

Kirkland, C.L., Hollis, J., Danišík, M., Petersen, J., Evans, N.J., and McDonald, B.J. (2017) 697 Apatite and titanite from the Karrat Group, Greenland; implications for charting the 698 thermal evolution of crust from the U-Pb geochronology of common Pb bearing phases. 699 Precambrian Research, 300, 107–120. 700 Kohn, M.J. (2017) Titanite Petrochronology. Reviews in Mineralogy and Geochemistry, 83, 701 702 419–441. Kohn, M.J., and Corrie, S.L. (2011) Preserved Zr-temperatures and U-Pb ages in high-grade 703 metamorphic titanite: Evidence for a static hot channel in the Himalayan orogen. Earth 704 and Planetary Science Letters, 311, 136–143. 705 Lamb, W.M. (1993) Retrograde deformation within the Carthage-Colton Zone as recorded by 706 fluid inclusions and feldspar compositions: tectonic implications for the southern 707 Grenville Province. Contributions to Mineralogy and Petrology, 114, 379–394. 708 Li, J.-W., Deng, X.-D., Zhou, M.-F., Liu, Y.-S., Zhao, X.-F., and Guo, J.-L. (2010) Laser 709 ablation ICP-MS titanite U-Th-Pb dating of hydrothermal ore deposits: A case study of 710 the Tonglushan Cu–Fe–Au skarn deposit, SE Hubei Province, China. Chemical Geology, 711 270, 56–67. 712 713 Lucassen, F., Dulski, P., Abart, R., Franz, G., Rhede, D., and Romer, R.L. (2010a) Redistribution of HFSE elements during rutile replacement by titanite. Contributions to Mineralogy and 714 Petrology, 160, 279–295. 715 716 Lucassen, F., Franz, G., Rhede, D., and Wirth, R. (2010b) Ti-Al zoning of experimentally grown 717 titanite in the system CaO-Al₂O₃-TiO₂-SiO₂-NaCl-H₂O-(F): Evidence for small-scale

fluid heterogeneity. American Mineralogist, 95, 1365.

718

- Lucassen, F., Franz, G., Dulski, P., Romer, R.L., and Rhede, D. (2011) Element and Sr isotope
- signatures of titanite as indicator of variable fluid composition in hydrated eclogite.
- 721 Lithos, 121, 12–24.
- Ludwig, K.R. (1998) On the Treatment of Concordant Uranium-Lead Ages. Geochimica et
- 723 Cosmochimica Acta, 62, 665–676.
- Ludwig, K (2009) SQUID 2: A User's Manual, rev. 12 Apr, 2009, 110 p.
- Ludwig, K.R. (2012) User's Manual for Isoplot 3.75: A Geochronlogical Toolkit for Microsoft
- 726 Excel, 75 p.
- Marsh, J.H., and Smye, A.J. (2017) U-Pb systematics and trace element characteristics in titanite
- from a high-pressure mafic granulite. Chemical Geology, 466, 403–416.
- McGregor, M., McFarlane, C.R.M., and Spray, J.G. (2019) In situ multiphase U–Pb
- geochronology and shock analysis of apatite, titanite and zircon from the Lac La Moinerie
- impact structure, Canada. Contributions to Mineralogy and Petrology, 174, 62.
- McLelland, J.M., Selleck, B.W., and Bickford, M.E. (2010) Review of the Proterozoic evolution
- of the Grenville Province, its Adirondack outlier, and the Mesoproterozoic inliers of the
- Appalachians. Geological Society of America Memoirs, 206, 21–49.
- Mezger, K., Pluijm, B. a. V.D., Essene, E.J., and Halliday, A.N. (1991a) Synorogenic Collapse:
- A Perspective from the Middle Crust, the Proterozoic Grenville Orogen. Science, 254,
- 737 695–698.
- Mezger, K., Rawnsley, C.M., Bohlen, S.R., and Hanson, G.N. (1991b) U-Pb Garnet, Sphene,
- Monazite, and Rutile Ages: Implications for the Duration of High-Grade Metamorphism
- and Cooling Histories, Adirondack Mts., New York. The Journal of Geology, 99, 415–
- 741 428.

Mezger, K., Pluijm, B.A. van der, Essene, E.J., and Halliday, A.N. (1992) The Carthage-Colton 742 Mylonite Zone (Adirondack Mountains, New York): The Site of a Cryptic Suture in the 743 Grenville Orogen? The Journal of Geology, 100, 630–638. 744 Mezger, K., Essene, E.J., van der Pluijm, B.A., and Halliday, A.N. (1993) U-Pb geochronology 745 of the Grenville Orogen of Ontario and New York: constraints on ancient crustal 746 747 tectonics. Contributions to Mineralogy and Petrology, 114, 13–26. Olierook, H.K.H., Taylor, R.J.M., Erickson, T.M., Clark, C., Reddy, S.M., Kirkland, C.L., Jahn, 748 I., and Barham, M. (2019) Unravelling complex geologic histories using U-Pb and trace 749 element systematics of titanite. Chemical Geology, 504, 105–122. 750 Papapavlou, K., Darling, J.R., Storey, C.D., Lightfoot, P.C., Moser, D.E., and Lasalle, S. (2017) 751 Dating shear zones with plastically deformed titanite: New insights into the orogenic 752 evolution of the Sudbury impact structure (Ontario, Canada). Precambrian Research, 291, 753 220-235. 754 Papapavlou, K., Darling, J.R., Moser, D.E., Barker, I.R., White, L.F., Lightfoot, P.C., Storey, 755 C.D., Dunlop, J., and EIMF (2018) U–Pb isotopic dating of titanite microstructures: 756 potential implications for the chronology and identification of large impact structures. 757 758 Contributions to Mineralogy and Petrology, 173, 82. Prowatke, S., and Klemme, S. (2005) Effect of melt composition on the partitioning of trace 759 760 elements between titanite and silicate melt. Geochimica et Cosmochimica Acta, 69, 695– 761 709. 762 Romer, R.L., and Rötzler, J. (2003) Effect of metamorphic reaction history on the U-Pb dating of 763 titanite. Geological Society, London, Special Publications, 220, 147–158.

Rubatto, D., and Scambelluri, M. (2003) U-Pb dating of magmatic zircon and metamorphic 764 baddeleyite in the Ligurian eclogites (Voltri Massif, Western Alps). Contributions to 765 Mineralogy and Petrology, 146, 341–355. 766 Schoene, B. (2014) 4.10-U–Th–Pb Geochronology. Treatise on Geochemistry, 4, 341–378. 767 Scibiorski, E., Kirkland, C.L., Kemp, A.I.S., Tohver, E., and Evans, N.J. (2019) Trace elements 768 769 in titanite: A potential tool to constrain polygenetic growth processes and timing. Chemical Geology, 509, 1–19. 770 Stacey, J.S., and Kramers, J.D. (1975) Approximation of terrestrial lead isotope evolution by a 771 two-stage model. Earth and Planetary Science Letters, 26, 207–221. 772 Stearns, M.A., Hacker, B.R., Ratschbacher, L., Rutte, D., and Kylander-Clark, A.R.C. (2015) 773 Titanite petrochronology of the Pamir gneiss domes: Implications for middle to deep 774 crust exhumation and titanite closure to Pb and Zr diffusion. Tectonics, 34, 784–802. 775 Stearns, M.A., Cottle, J.M., Hacker, B.R., and Kylander-Clark, A.R.C. (2016) Extracting thermal 776 histories from the near-rim zoning in titanite using coupled U-Pb and trace-element depth 777 profiles by single-shot laser-ablation split stream (SS-LASS) ICP-MS. Chemical 778 Geology, 422, 13–24. 779 780 Stern, Robert (1997) The GSC sensitive high resolution ion microprobe (SHRIMP): analytical techniques of zircon U–Th–Pb age determinations and performance evaluation. 781 782 Geological Survey of Canada Report, 10, 1–31. 783 Storey, C.D., Jeffries, T.E., and Smith, M. (2006) Common lead-corrected laser ablation ICP-

MS U-Pb systematics and geochronology of titanite. Chemical Geology, 227, 37–52.

784

Storey, C.D., Smith, M.P., and Jeffries, T.E. (2007) In situ LA-ICP-MS U-Pb dating of 785 metavolcanics of Norrbotten, Sweden: Records of extended geological histories in 786 complex titanite grains. Chemical Geology, 240, 163–181. 787 Streepey, M., E. L. Johnson, K. Mezger, and B. A. van der Pluijm (2001) Early History of the 788 Carthage-Colton Shear Zone, Grenville Province, Northwest Adirondacks, New York 789 790 (U.S.A.). The Journal of Geology, 109, 479–492. Tera, F., and Wasserburg, G.J. (1972) U-Th-Pb systematics in three Apollo 14 basalts and the 791 problem of initial Pb in lunar rocks. Earth and Planetary Science Letters, 14, 281–304. 792 793 Tera, F., and Wasserburg, G.J. (1974) U-Th-Pb systematics on lunar rocks and inferences about lunar evolution and the age of the moon. In Lunar and Planetary Science Conference 794 Proceedings Vol. 5, pp. 1571–1599. 795 Tiepolo, M., Oberti, R., and Vannucci, R. (2002) Trace-element incorporation in titanite: 796 constraints from experimentally determined solid/liquid partition coefficients. Chemical 797 Geology, 191, 105–119. 798 Timms, N.E., Pearce, M.A., Erickson, T.M., Cavosie, A.J., Rae, Auriol S. P., Wheeler, J., 799 Wittmann, Axel, Ferrière, Ludovic, Poelchau, Michael H., Tomioka, Naotaka, and others 800 801 (2019) New shock microstructures in titanite (CaTiSiO5) from the peak ring of the Chicxulub impact structure, Mexico. Contributions to Mineralogy and Petrology, 174, 38. 802 803 Verts, L.A., Chamberlain, K.R., and Frost, C.D. (1996) U-Pb sphene dating of metamorphism: 804 the importance of sphene growth in the contact aureole of the Red Mountain pluton, 805 Laramie Mountains, Wyoming. Contributions to Mineralogy and Petrology, 125, 186– 199. 806

807	Williams, I.S. (1998) U-Th-Pb geochronology by ion microprobe. Reviews in Economic
808	Geology, 7, 1–35.
809	Wohlgemuth-Ueberwasser, C.C., Tegner, C., and Pease, V. (2017) LA-Q-ICP-MS apatite U/Pb
810	geochronology using common Pb in plagioclase: Examples from layered mafic
811	intrusions. American Mineralogist, 102, 571–579.
812	Zhang, X.Y., Cherniak, D.J., and Watson, E.B. (2006) Oxygen diffusion in titanite: Lattice
813	diffusion and fast-path diffusion in single crystals. Chemical Geology, 235, 105–123.
814	

Figure Captions 815 Figure 1. Post-analysis images of U-Pb LA-ICP-MS and SHRIMP analysis pits at a similar scale. 816 Both sets of analysis pits have similar diameters, 35-40 µm. SHRIMP pits are 2-3 µm deep; LA-817 ICP-MS pits are 15 µm deep. 818 819 820 Figure 2. Total LA-ICP-MS and SHRIMP U-Pb titanite datasets, colored by grain 'Type' as determined by microstructural setting (Bonamici et al., 2014; 2015). The LA-ICP-MS dataset is 821 more extensive (n = 280) than the SHRIMP dataset (n = 101) because of the shorter analysis 822 time. 823 824 Figure 3. Total Pb/U plots for each Adirondack titanite grain. Grain designations are listed in 825 upper right corner of each plot with the Type in parentheses behind. See Table 1 for grain Type 826 explanations. LA-ICP-MS data shown in gray; SHRIMP data shown in black. Constrained 3D 827 828 linear regressions are projected into the 2D space of the Tera-Wasserburg diagram. Lower concordia intercepts and MSWDs for constrained 3D and 2D regressions are given for each 829 grain. Leftmost column contains Type-1 and -2 grains, which show generally small U/Pb ratio 830 831 spread and highly clustered analyses. Center column contains Type-3 grains, which show greater U/Pb variations. The rightmost column contains Type-4 grains showing the largest spread in 832 833 U/Pb ratios. 834 835 Figure 4. Results of 3D linear isochron regressions (Ludwig, 2012) for individual Adirondack titanite grains, showing large uncertainties and relatively poor age constraints provided by this 836 837 type of analysis. See also Figure 3 and Table 1. (A) Concordia-intercept ages and 2SD

uncertainties from regressions with constrained Pbi ²⁰⁷Pb/²⁰⁶Pb. Light gray fields show the known age ranges for the Shawinigan and Ottawan phases of the Grenville orogenic cycle for reference. (B) Lower intercepts and 2SD uncertainties, in the Tera-Wasserburg plane, of unconstrained regressions. Within large uncertainties, all but one grain (HA12B) give lower intercepts the overlap concordia. All regressions of SHRIMP data return MSWD values greater than 2. Approximate ages for the Shawinigan and Ottawan phases are indicated on the concordia for reference.

Figure 5. Comparison of individually Pbi-corrected U-Pb dates for a subset of Adirondack titanite grains that were analyzed by both LA-ICP-MS and SHRIMP. Traverses show the spatial variations in Pbi-corrected ²³⁸U/²⁰⁶Pb dates. Profiles are generated using the preferred Pbi-correction for each analytical technique—207 method for LA-ICP-MS and 204-method for SHRIMP. Vertical bars show average, external 1σ uncertainties for SHRIMP (red) and LA-ICP-MS (blue). Dashed horizontal lines show mean concordia-intercept ages from 3D linear isochron regressions; note that uncertainties on these regression ages are not shown but are generally large (see Fig. 4). U-Pb profiles for all grains in this study can be found in Supplemental Figures S1 through S13.

Figure 6. Plot of total ²⁰⁷Pb/²⁰⁶Pb vs. total ²⁰⁴Pb/²⁰⁶Pb measured in Harrisville titanite by LA-ICP-MS (blue) and SHRIMP (red). See text for discussion.

Figure 7. Schematic diagrams showing the behavior of U-Pb data on a Tera-Wasserburg diagram. (A) Selected paths showing the ingrowth of radiogenic Pb in the absence of Pb_i as

function of various starting U isotope compositions. Topmost path shows ingrowth trajectory for a titanite grain crystallized at the time of Earth formation with the primodial (meteoritic) U isotope composition. (B) Evolution of a mixing line (isochron) between Pb* and Pb_i with 207 Pb/ 206 Pb = 0.96. Black line with the steepest slope represents the present-day isochron. Gray lines with negative slopes show the position of the isochron at different arbitrary times during its evolution from its initial to its present-day position. Gray lines with positive slopes show ingrowth curves for Pb* mixed with variable proportions of Pb_i. Pb_i composition is shown by the horizontal dashed line. (C) Same as B with a different isochron evolution superimposed (blue lines), demonstrating the effect of later titanite (re)crystallization with a different, more radiogenic Pb_i (207 Pb/ 206 Pb = 0.6). (D) Schematic representation of Pb ingrowth trajectories for titanite suffering open-system modification of its U/Pb ratio. Thin colored lines are normal ingrowth trajectories (with varying proportions of Pb_i); heavier arrows simulate instantaneous change in U/Pb ratio by either recent or ancient open-system event. Subsequently, Pb ingrowth returns to closed-system behavior (thin lines). (E) Schematic representation of the U-Pb data arrays expected in the case of open-system U/Pb ratio modification, as demonstrated in D.

Figure 8. U-Pb analyses with color scaling showing covariation with additional isotopic data. (A) SHRIMP data and (B) LA-ICP-MS data with color scaling showing total ²⁰⁴Pb/²⁰⁶Pb. The transition from warm to cool colors toward concordia is consistent with decreasing relative abundance of Pb_i. (C) SHRIMP data and (D) LA-ICP-MS data with color scaling showing 204-corrected date. Comparison with A and B suggests that for a given ²⁰⁴Pb/²⁰⁶Pb value (Pb_i abundance), variation in Pb_i-corrected dates reflects variation in U/Pb ratio. Only Type 1 and Type 2 data, which retain evidence for oxygen isotope and Pb diffusion (Bonamici et al. 2014; 2015), are shown in B and D.

Figure 9. Quantitative models showing the effect of Pb loss on U-Pb systematics for titanite with Pb_i on the Terra-Wasserberg diagram. Model is constructed to simulate possible scenarios for the Harrisville titanite grains: initial crystallization at 1150 Ma with low Pb_i followed by Pb loss shortly after crystallization at 1050 Ma (orange curve) or Pb loss long after crystallization at 650 Ma (green curve). Modeling details in Supplemental Materials. (A) Ingrowth curves showing full ingrowth trajectories, including Pb loss events. (B) Expanded region of A showing where evolution curves end (X's), relative to the 1150 Ma and 1050 Ma isochrons, and depending on the timing of Pb loss.

895 Appendix

Stacey and Kramers (1975) determined modern-day crustal average Pb isotope ratios to be

206Pb/204Pb = 18.70, 207Pb/204Pb = 15.63, and 208Pb/204Pb = 38.63, based on Pb isotopic data from

"conformable" galena. They then fitted a two-stage Pb evolution curve, the second stage having

μ = 238U/204Pb = 9.74. In practice, Pb_i ratios based on the Stacey and Kramers (1975) model can

be calculated for materials younger than 3.7 Ga from equations 1 and 2 below, using the modernday crustal average Pb isotope ratios and an approximate age (Stacey and Kramers model Pb

ratios are superscipted SK).

903

904
$$\left(\frac{^{206}Pb}{^{204}Pb}\right)_{i}^{SK} = \left(\frac{^{206}Pb}{^{204}Pb}\right)_{today}^{SK} - m\left(e^{'238^{t}} - 1\right)$$
 [eq.1]

905
$$\left(\frac{^{207}Pb}{^{204}Pb}\right)_{i}^{SK} = \left(\frac{^{207}Pb}{^{204}Pb}\right)_{today}^{SK} - \frac{1}{137.82}m(e^{^{\prime}235^{t}} - 1) \qquad [eq. 2]$$

906

The 204 method initial Pb correction (Stern, 1997) subtracts the initial Pb fraction (^{204c}f₂₀₆), calculated using Stacey and Kramers (1975) Pb_i ratios, from the total measured ²⁰⁶Pb/²³⁸U to determine the radiogenic ²⁰⁶Pb/²³⁸U ratio.

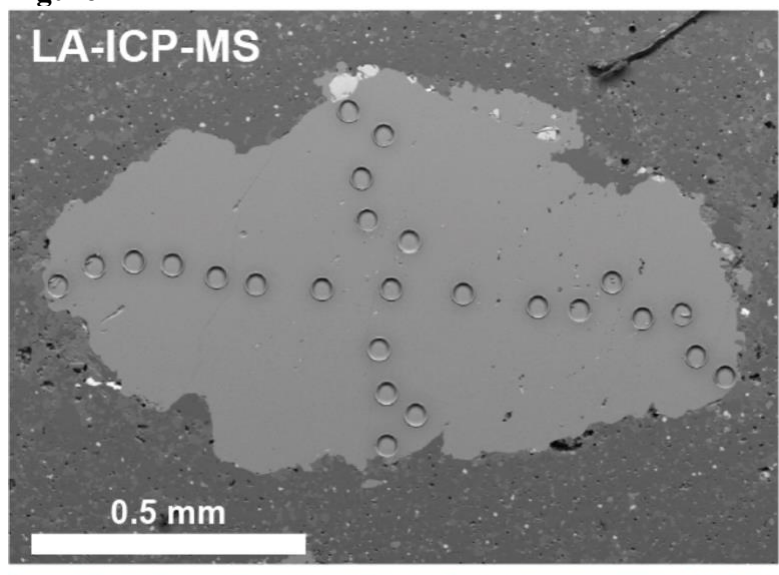
912

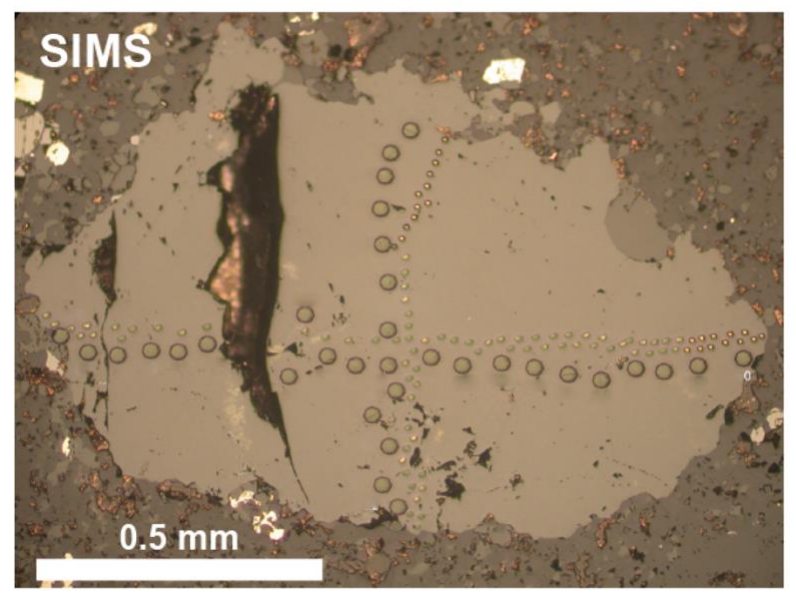
The 207 method Pb_i correction (Stern, 1997) subtracts the initial Pb fraction (^{207c}f₂₀₆), calculated using Stacey and Kramers (1975) Pb_i values and a starting guess or "expected" radiogenic ²⁰⁷Pb/²⁰⁶Pb ratio, from the total measured ²⁰⁷Pb/²⁰⁶Pb to determine the corrected radiogenic ²⁰⁷Pb/²⁰⁶Pb ratio.

917
$$\frac{207c}{f_{206}} = \frac{\frac{206}{Pb_{i}}}{\frac{206}{Pb_{total}}} = \frac{\left(\frac{206}{Pb}\right)^{unknown}_{measured} - \left(\frac{206}{207}\frac{Pb^{*}}{Pb^{*}}\right)^{unknown}_{expected}}{\left(\frac{206}{207}\frac{Pb}{Pb}\right)^{SK}_{i} - \left(\frac{206}{207}\frac{Pb^{*}}{Pb^{*}}\right)^{unknown}_{expected}}$$
 [eq.5]

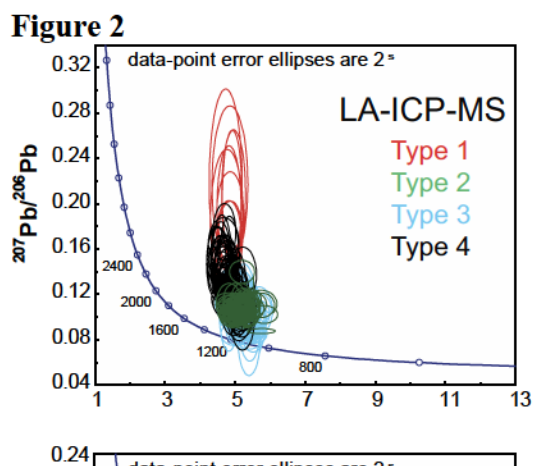
918
$$f_{207} = {}^{207c} f_{206} \left(\frac{({}^{207}Pb/{}^{206}Pb)_{i}^{SK}}{({}^{207}Pb/{}^{206}Pb)_{measured}^{NN}} \right) [eq.6]$$

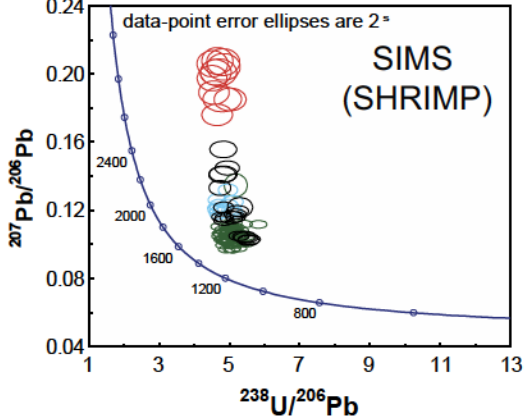
Figure 1

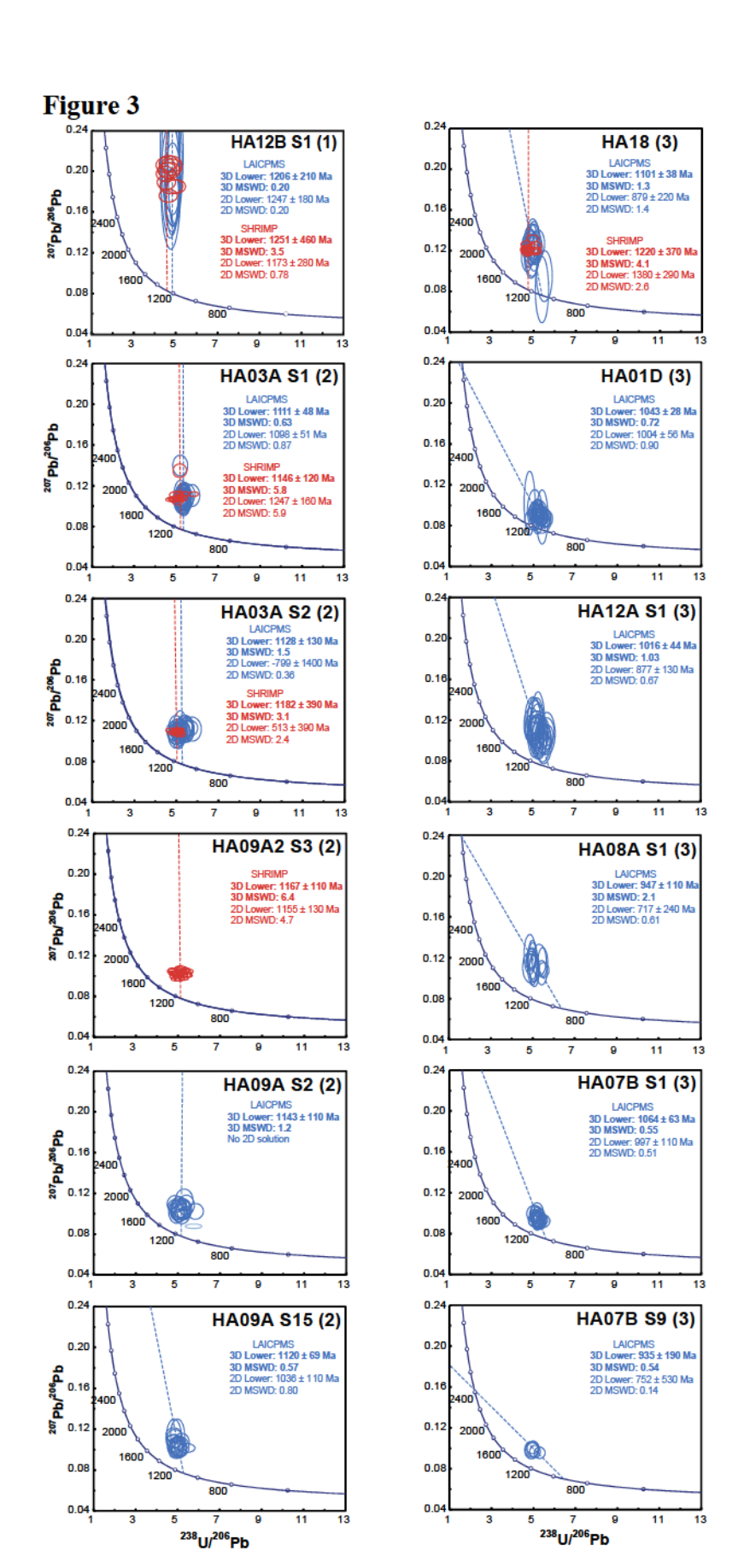












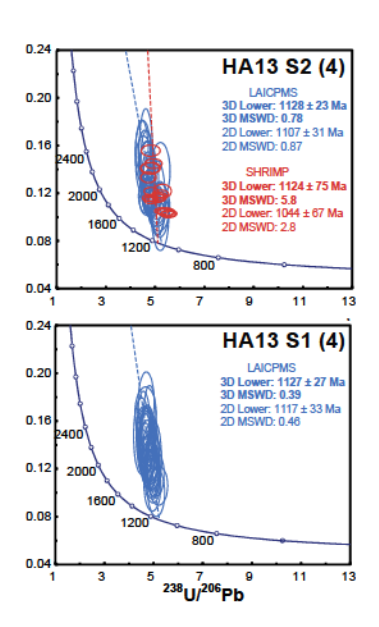
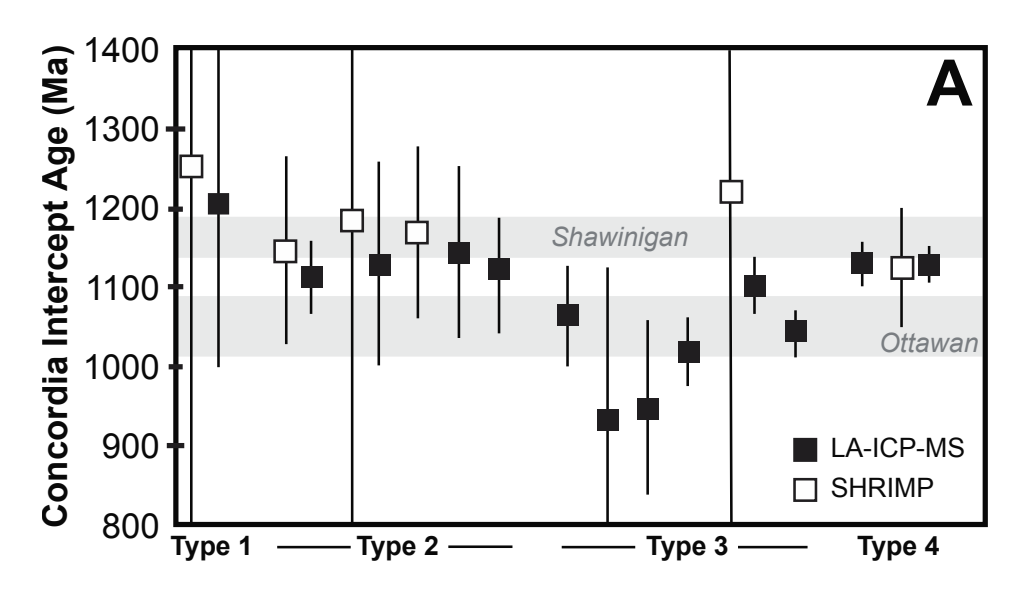


Figure 4



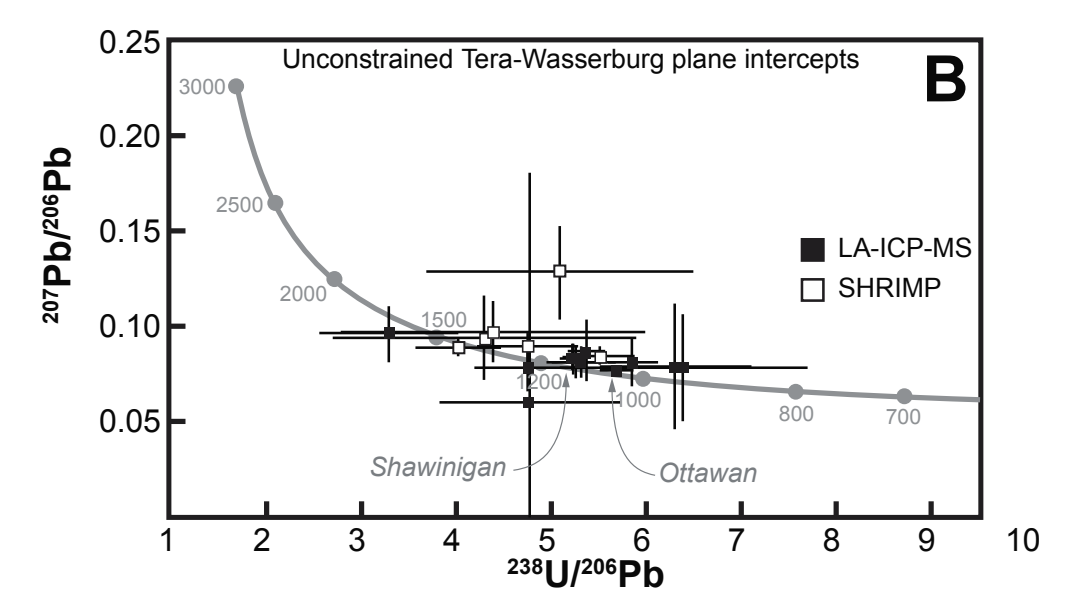
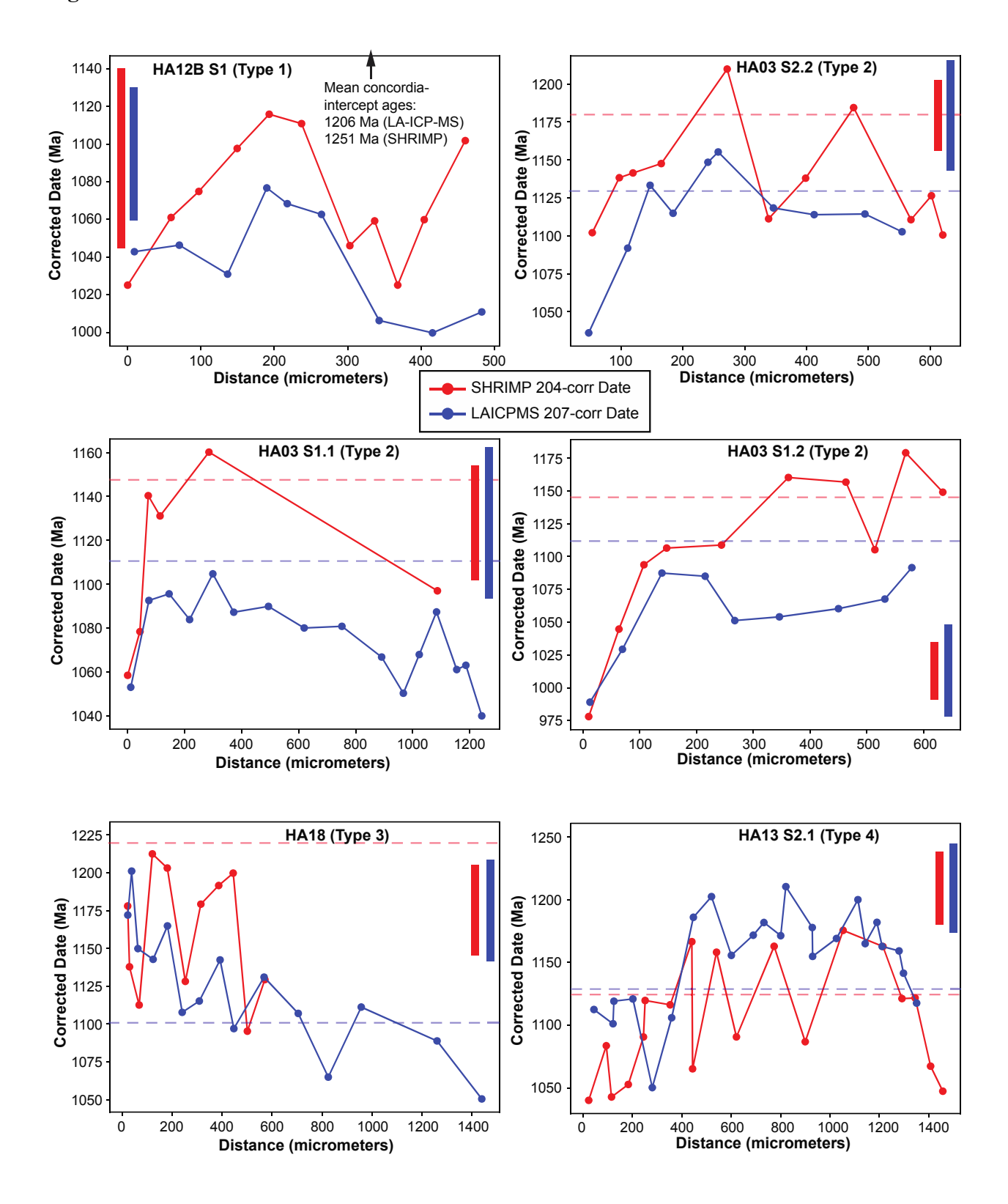
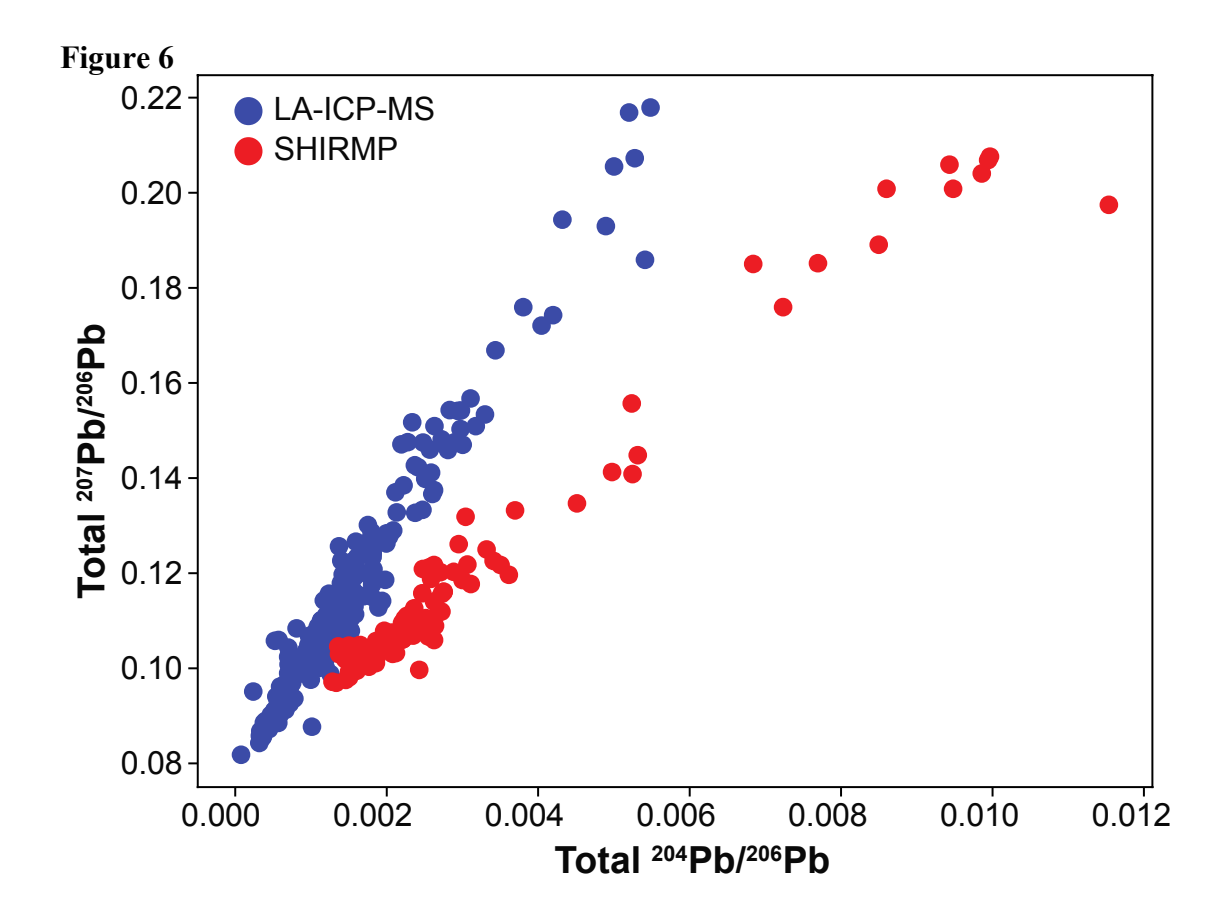


Figure 5





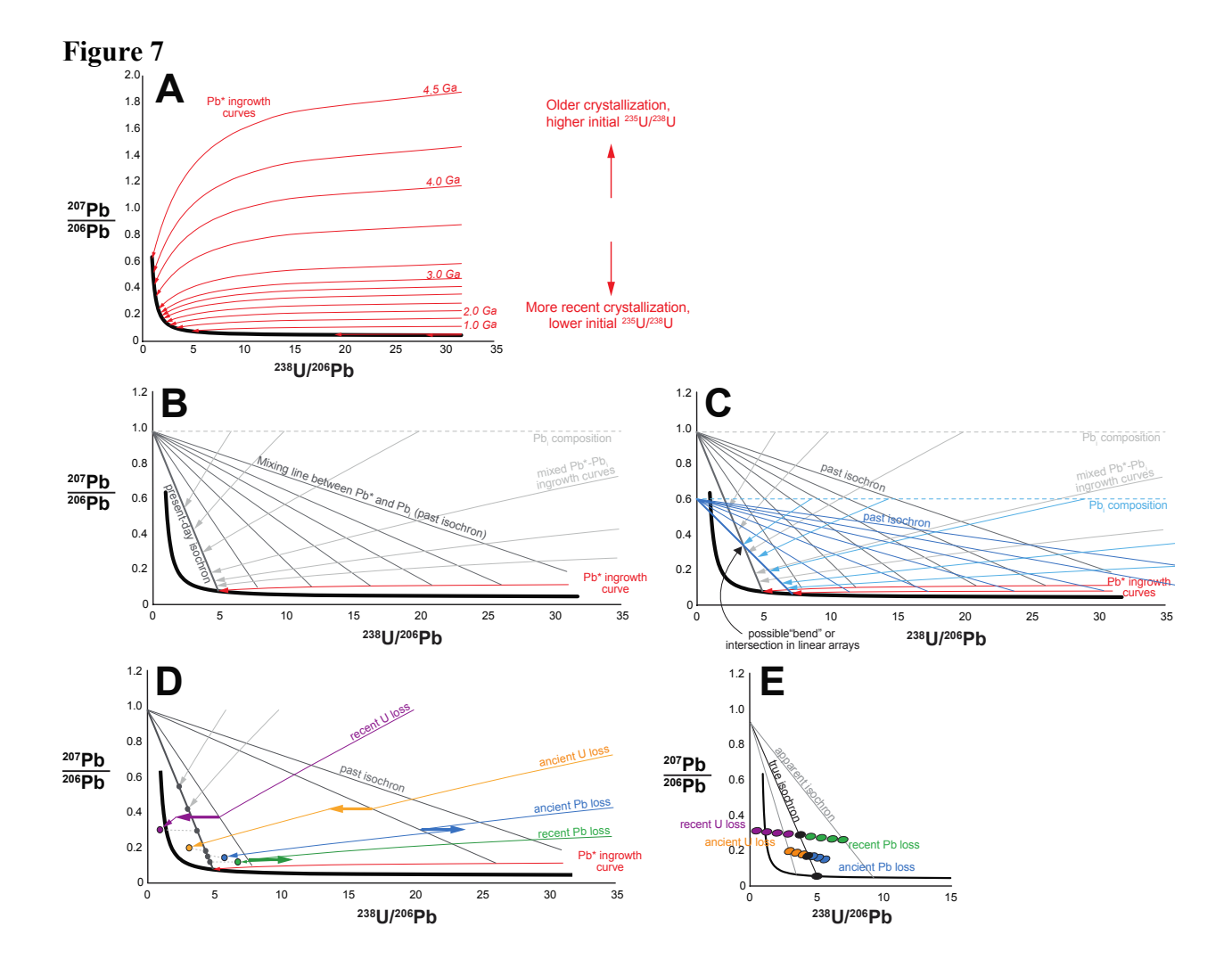


Figure 8

